JOURNAL OF AIRCRAFT
Vol. 51, No. 2, March–April 2014

Sonic-Boom Mitigation Through Aircraft Design and Adjoint Methodology

Sriram K. Rallabhandi*
National Institute of Aerospace, Hampton, Virginia 23666
Eric J. Nielsen†
NASA Langley Research Center, Hampton, Virginia 23681
and
Boris Diskin‡
National Institute of Aerospace, Hampton, Virginia 23666

DOI: 10.2514/1.C032189

This paper presents a novel approach to design of the supersonic aircraft outer mold line by optimizing a A-weighted loudness-based objective of the sonic-boom signature predicted on the ground. The optimization process uses the sensitivity information obtained by coupling the discrete adjoint formulations for the augmented Burgers equation and computational-fluid-dynamics equations. This coupled formulation links the loudness of the ground boom signature to the aircraft geometry, thus allowing efficient shape optimization for the purpose of minimizing the loudness. The accuracy of the adjoint-based sensitivities is verified against sensitivities obtained using an independent complex-variable approach. The adjoint-based optimization methodology is applied to a configuration previously optimized using alternative state-of-the-art optimization methods and produces additional loudness reduction. The results of the optimizations are reported and discussed.

Nomenclature

A^n, B^n	=	matrices during the first relaxation process
A_2^n, B_2^n	=	matrices during the second relaxation process
A_3^n, B_3^n	=	matrices during the absorption process
C_ν	=	nondimensional dispersion
c_0	=	ambient speed of sound, m/s
D	=	vector of design variables
G	=	ray-tube area
$\mathbf{G}$	=	grid equations
I_N	=	objective/cost function for adjoint calculation
k_n	=	scaling factor due to ray-tube spreading and stratification
L	=	Lagrangian
N	=	number of steps during propagation
p, P	=	pressure waveform during propagation
$\boldsymbol{Q}$	=	flow solution vector
q, r, t	=	intermediate pressure waveforms
$\mathbf{R}$	=	discrete flow equations
$\mathbf{T}$	=	transformation mapping flow solution to a desired off-body pressure distribution
$\boldsymbol{X}$	=	mesh solution vector
β	=	$1 + \frac{\gamma-1}{2}$
Γ	=	nondimensional thermoviscous parameter
γ	=	ratio of specific heats, 1.4
θ_ν	=	nondimensional relaxation time parameter
Λ_b	=	adjoint variables corresponding to boom equations
Λ_f	=	adjoint variables corresponding to flow equations
Λ_g	=	adjoint variables corresponding to grid equations
λ_n,β_n,$\gamma_{0,n}$, $\gamma_{1,n}$	=	adjoint vectors
ρ_0	=	ambient density
σ	=	nondimensional distance
τ	=	nondimensional time
τ'	=	retarded time

Subscript

n	=	propagation iteration counter

I. Introduction

Development of novel, efficient, and reliable methods to design supersonic aircraft for the purpose of sonic-boom mitigation remains one of the most important steps in the conceptual and preliminary design stages. Since the 1960s, researchers [1–3] realized the importance of aircraft shaping in reducing the sonic-boom impact. The Shaped Sonic Boom Demonstrator [4] program verified, via flight testing, that aircraft shaping is an effective strategy for changing the boom signature on the ground. Since this groundbreaking study, there have been persistent efforts directed toward achieving better designs (e.g., Quiet Spike [5]) to reduce the boom footprint.

Although there have been studies [6] that show some promise toward achieving sonic-boom mitigation without the use of sensitivity information, design approaches based on sensitivity of pressure distributions to the aircraft shape offer an effective and theoretically sound way to reduce the adverse impact of sonic boom. Adjoint-based methods provide effective tools to compute sensitivities of various aerodynamic quantities to many shape design parameters. Several studies [7,8] demonstrated capabilities of adjoint-based methods to optimize near-field sonic-boom waveforms.

Almost all adjoint-based shape optimization exercises in the literature for sonic-boom minimization use near-field target matching. The main reason for this is that near-field matching is not only an easier and more intuitive problem compared to using cost functionals on the ground but also the only approach available to researchers to perform high-fidelity shape optimization for boom mitigation. For near-field targets, there is a one-to-one

Presented as Paper 2012-3220 at the 30th Applied Aerodynamics Conference, New Orleans, LA, 25–28 June 2012; received 1 November 2012; revision received 15 June 2013; accepted for publication 15 September 2013; published online 5 March 2014.

*Senior Research Engineer. Senior Member AIAA.
†Research Engineer, Computational AeroSciences Branch. Senior Member AIAA.
‡Fellow; currently Visiting Associate Professor, Mechanical and Aerospace Engineering Department, University of Virginia, Charlottesville, VA 22903. Associate Fellow AIAA.

correspondence between the shocks and expansions in the off-body waveform and the geometry. This one-to-one correspondence is lost during propagation to the ground due to shock coalescence and other atmospheric phenomena. Although matching a near-field target is one possible approach for boom mitigation, it may be beneficial to pose this problem from the perspective of ground metrics.

Even though optimization based on ground-level objectives is less intuitive, working directly with ground metrics is desirable because they represent physically measurable quantities that are used in boom acceptability studies. Previous work along this direction [9] used a high-fidelity design approach for the purpose of ground-target signature matching using adjoint-based shape optimization. Although directly optimizing for better ground signatures is a step closer to the ultimate design intent than optimizing near-field pressure waveforms, it is still limited in applicability. The primary reason for this is that specifying a suitable ground target for a chosen geometry parameterization scheme is challenging. Merely smoothing a baseline ground signature or specifying a smooth sine-wave-like signature can lead to situations where the optimizer may not be able to reach this target simply because the prescribed ground target may not be in the range space of the chosen parameterization. Moreover, the minimization of the sum of squared errors between the target and design signatures does not necessarily translate to reduced loudness values. This is because loudness values depend on the frequency content of the ground signature and cannot be captured by the sum of squared errors. To overcome these problems, this paper uses a metric based on sonic-boom ground signature loudness as the optimization objective. This guarantees that the signature obtained after optimization will have a loudness value lower than the signature of the baseline configuration. This cannot be guaranteed for ground target matching. The methodology described in this study does not necessarily replace current state-of-the-art approaches; it complements them by providing a useful tool for additional shape optimization and allowing the designer to look at the design space through a different prism. The adjoint-based methodology introduced in this paper is the first rigorous methodology that allows inclusion of integrated ground level objectives in design optimization for sonic-boom mitigation; it is unique in this respect.

The main goals of this paper are 1) to formulate the loudness adjoint problem, 2) predict the sensitivities of a loudness (A-weighted loudness) objective with respect to selected design variables, 3) couple boom-adjoint method with an adjoint computational fluid dynamics (CFD) solver, and 4) demonstrate the functionality using an aircraft shape optimization exercise.

II. Mathematics of Boom Adjoint

This section presents the mathematics of boom-adjoint methodology. The primal problem refers to the augmented Burgers's propagation [10] and is given in Eq. (1):

$$\frac{\partial P}{\partial \sigma} = P\frac{\partial P}{\partial \tau} + \frac{1}{\Gamma}\frac{\partial^2 P}{\partial \tau^2} + \Sigma_\nu \frac{C_\nu \frac{\partial^2}{\partial \tau^2}}{1+\theta_\nu \frac{\partial}{\partial \tau}} P - \frac{1}{2G}\frac{\partial G}{\partial \sigma}P + \frac{1}{2\rho_0 c_0}\frac{\partial(\rho_0 c_0)}{\partial \sigma}P \tag{1}$$

An operator splitting scheme [10,11] is used to solve a set of five equations under the assumption that, if the time step is small, the error induced by splitting is small. Equation (2) represents the effect of first relaxation and scaling due to ray-tube area spreading and stratification. The matrices included in these equations are provided in the Appendix. Based on the discretization scheme used, the matrices are tridiagonal; hence, the Thomas algorithm [12] may be used to solve the system efficiently. Because there are two relaxation phenomena corresponding to oxygen and nitrogen, Eqs. (2) and (3) are each solved using their respective values for C_ν and θ_ν:

$$A^n q_n = k_n B^n p_{n-1} \tag{2}$$

$$A_2^n r_n = B_2^n q_n \tag{3}$$

For the absorption equation, a Crank–Nicholson scheme is used for advancing the pressure in time. Using this discretization scheme, the absorption phenomenon also transforms into a tridiagonal matrix problem as given in Eq. (4), which is solved to obtain t_n:

$$A_3^n t_n = B_3^n r_n \tag{4}$$

The nonlinear equation is solved using the Poisson solution and is dependent on the solution from the absorption equation as given in Eq. (5). In this equation, t_n is a function with two arguments, the propagation distance σ_n and the time coordinate; t_n can be thought of as a matrix such that $t_{n,i}$ represents the σ_nth row and τ_ith column. This retarded time equation is solved via re-interpolation as shown in Eq. (6), where τ' is the retarded coordinate given by $\tau'_{n,i} = \tau_i - t_{n,i}\Delta\sigma_n$, $\Delta\sigma_n = \sigma_n - \sigma_{n-1}$, and j is an index such that $\tau'_{n,i-1} < \tau_j < \tau'_{n,i}$. Expanding the terms results in the discretized equation for the nonlinear part of the Burgers's equation primal problem as given in Eq. (7):

$$p(\sigma_n, \tau_i) = t_n(\sigma_n, \tau_i + t_{n,i}\Delta\sigma_n) \tag{5}$$

$$p_{n,j} = t_{n,i-1} + \frac{t_{n,i} - t_{n,i-1}}{\tau'_{n,i} - \tau'_{n,i-1}}(\tau_j - \tau'_{n,i-1}) \tag{6}$$

$$p_{n,j} = t_{n,i-1} + \frac{t_{n,i} - t_{n,i-1}}{\Delta\tau - (t_{n,i} - t_{n,i-1})\Delta\sigma_n}[\tau_j - \tau_{i-1} + t_{n,i-1}\Delta\sigma_n] = f_{n,j} \tag{7}$$

The ray-tube spreading and atmospheric stratification are simply scaling terms; these are included in the k factor in Eq. (2). For the solution of the augmented Burgers's equation, Eqs. (2–4) and (7) are solved repeatedly, in that order, for $n = 1 \ldots N$ time steps, and at each stage, the pressure is updated, while also successively updating intermediate values: r, q, and t.

The discrete adjoint equations are derived in this section based on a similar implementations given by Nielsen et al. [13] and Rallabhandi [9]. If D is the vector of design variables and I_n is the objective function, then the Lagrangian corresponding to this objective may be written as in Eq. (8). Taking the derivative of the Lagrangian with respect to D results in Eq. (9), where it has been assumed that the objective does not depend explicitly on the intermediate pressure vectors r, q, and t. Furthermore, the matrices themselves do not depend on the initial pressure profile:

$$\begin{aligned} L(p,q,r,t,D) = {} & I_N(p_N, D) + \sum_{n=2}^{N} \gamma_{0,n}^T [A^n q_n - k_n B^n p_{n-1}]\Delta\sigma_n \\ & + \sum_{n=1}^{N} \gamma_{1,n}^T [A_2^n r_n - B^n q_n]\Delta\sigma_n + \sum_{n=1}^{N} \beta_n^T [A_3^n t_n - B_3^n r_n]\Delta\sigma_n \\ & + \sum_{n=1}^{N} \lambda_n^T [p_n - f^n(t_n, D)]\Delta\sigma_n + \gamma_{0,1}^T [A^1 q_1 - k_1 B^1 D]\Delta\sigma_n \end{aligned} \tag{8}$$

$$\begin{aligned} \frac{\mathrm{d}L}{\mathrm{d}D} = {} & \left[\frac{\partial I_N}{\partial D} + \frac{\partial I_N}{\partial p_N}\frac{\partial p_N}{\partial D}\right] + \sum_{n=2}^{N} \gamma_{0,n}^T \left[A^n \frac{\partial q_n}{\partial D} - k_n B^n \frac{\partial p_{n-1}}{\partial D}\right]\Delta\sigma_n \\ & + \sum_{n=1}^{N} \gamma_{1,n}^T \left[A_2^n \frac{\partial r_n}{\partial D} - B_2^n \frac{\partial q_n}{\partial D}\right]\Delta\sigma_n + \sum_{n=1}^{N} \beta_n^T \left[A_3^n \frac{\partial t_n}{\partial D} - B_3^n \frac{\partial r_n}{\partial D}\right]\Delta\sigma_n \\ & + \sum_{n=1}^{N} \lambda_n^T \left[\frac{\partial p_n}{\partial D} - \frac{\partial f_j^n}{\partial t_n}\frac{\partial t_n}{\partial D}\right]\Delta\sigma_n + \gamma_{0,1}^T \left[A^1 \frac{\partial q_1}{\partial D} - k^1 B^1\right]\Delta\sigma_n \end{aligned} \tag{9}$$

Collecting the $\partial p_n/\partial D$, $\partial t_n/\partial D$, $\partial r_n/\partial D$, and $\partial q_n/\partial D$ terms from Eq. (9) and equating them to zero results in a system of four adjoint equations that is solved iteratively backward in time. Collecting all of the $\partial p_n/\partial D$ terms and simplifying yields Eq. (10). Similarly, collecting the $\partial t_n/\partial D$, $\partial r_n/\partial D$, and $\partial q_n/\partial D$ terms, we have Eqs. (11–13), respectively. The adjoint solution process involves solving Eqs. (10–13) iteratively. Equation (10) is solved initially by assuming $\gamma_{0,N+1} = 0$ because there are no "$N + 1$" terms in our primal propagation problem. The intermediate adjoints are successively updated and solved. The primal problem is solved first, and relevant pressure vectors are stored for use in the adjoint process:

$$\lambda_n^T = -\frac{\partial I_N}{\partial p_N} + \gamma_{0,n+1}^T k_{n+1} B^{n+1} \tag{10}$$

$$\beta_n^T A_3^n = \lambda_n^T \frac{\partial f_j^n}{\partial t_n} \tag{11}$$

$$\gamma_{1,n}^T A_2^n = \beta_n^T B_3^n \tag{12}$$

$$\gamma_{0,n}^T A^n = \gamma_{1,n}^T B_2^n \tag{13}$$

III. Problem Setup

The ultimate objective of shape optimization in this study is the reduction of the sonic-boom impact at the ground level through the use of A-weighted loudness. Although it is desirable to use the perceived loudness level as the ground level metric to perform adjoint-based shape optimization, there was no easy way to compute the sensitivity of this metric with respect to the ground signature that is needed in adjoint-based design optimization. A-weighted loudness computation, on the other hand, offers an analytical calculation procedure that can be readily differentiated for generating required sensitivities and therefore amenable to adjoint-based shape design. In addition, the A-weighted loudness is well correlated [14] with the perceived loudness values. If a technique were to become available that would allow computation of perceived loudness level sensitivities, then the current methodology could be readily extended to minimize a cost functional that is a function of the perceived loudness on the ground.

The objective function used in this study is given in Eq. (14), where target A-weighted loudness value is chosen as 56.0. Although the objective chosen could just be the A-weighted loudness, a quadratic form was chosen to make the optimization problem convex and therefore well behaved. The derivative of the cost function [Eq. (15)] can be used in Eq. (10) to start the adjoint calculation process. The partial derivative of the A-weighted loudness with respect to the ground pressure profile is needed for this calculation. A time-domain version of the A-weighted loudness calculation procedure based on Butterworth digital filters [15] was obtained from Gulfstream. This code was then numerically differentiated and modified to yield loudness sensitivity terms in addition to the loudness values:

$$I_N = (\mathrm{dBA}_{\mathrm{design}} - \mathrm{dBA}_{\mathrm{target}})^2 \tag{14}$$

$$\frac{\partial I_N}{\partial p_N} = 2.0(\mathrm{dBA}_{\mathrm{design}} - \mathrm{dBA}_{\mathrm{target}}) \frac{\partial \mathrm{dBA}_{\mathrm{design}}}{\partial p_N} \tag{15}$$

To verify that the loudness sensitivity values are correct, a complex variable version of the loudness calculation procedure was developed. The complex variable approach [16,17] has been applied in several other gradient verifications. The main advantage of the complex variable method is that true second-order accuracy is achieved by selecting step sizes without incurring subtractive cancellation errors typically present in real-valued finite differences. Table 1 shows the comparison of the loudness sensitivity values computed using the analytically differentiated loudness code and the complex version of the code for arbitrarily selected indices in the ground signature. Here, it can be seen that the values match to up to 14 decimal places, thus verifying that the loudness sensitivity values are accurate for our purposes.

Table 1 Comparison of the direct and complex variable loudness gradients

Grid point	Direct gradient	Complex variable gradient
55	−1.7810273118252038	−1.7810273118252047
328	−0.005301921655030	−0.005301921655029
800	−0.002079879894158	−0.002079879894158
855	0.000376554607869	0.000376554607869

Other cost functions can be included into the optimization framework as well. These could either be matching a target ground signature as in Eq. (16) or a combination of A-weighted loudness and target ground signature as in Eq. (17) or just the A-weighted loudness as in Eq. (18) or other appropriate combinations of undertrack and off-track signature metrics. For each chosen cost functional, Eq. (10) needs to be updated to obtain the adjoint solutions:

$$I_{2,N} = \sum_{i=1}^{M} [p_N^i - p_t^i]^2 \tag{16}$$

$$I_{3,N} = (\mathrm{dBA}_{\mathrm{design}} - \mathrm{dBA}_{\mathrm{target}})^2 + \sum_{i=1}^{M} [p_N^i - p_t^i]^2 \tag{17}$$

$$I_{4,N} = \mathrm{dBA}_{\mathrm{design}} \tag{18}$$

A. Gradient Calculation

For adjoint solutions satisfying Eqs. (10–13), the only remaining term is the last term shown in Eq. (19). After the adjoint equations are solved, the last solution of Eq. (13) is multiplied with the scaling factor and the tridiagonal matrix of the first relaxation process to generate the gradient values needed for optimization:

$$\frac{\mathrm{d}L}{\mathrm{d}D} = -\gamma_{0,1}^T k_1 B^1 \Delta\sigma_1 \tag{19}$$

B. Verification of Adjoint Sensitivities

Boom propagation starts by obtaining off-body pressure distributions of the baseline concept using CFD. The propagation process discretizes these CFD off-body waveforms into desired uniform spacing grids and extrapolates these toward the ground. During this extrapolation, intermediate waveforms are stored for use in the adjoint method. The adjoint method is run using the cost function described in Eq. (14). To verify the accuracy of the adjoint implementation, comparisons are made with gradients generated through the use of a complex variable approach. The propagation process is modified to work with complex variables, and the derivatives of the loudness with respect to the design variables (off-body pressure distribution; in this case) are calculated using an imaginary step size of 10^{-50}. Table 2 compares the adjoint gradients against the complex variable gradients for some arbitrary grid point locations. It is seen that the results using adjoint implementation exhibit excellent agreement with the complex-variable approach. This verifies that the gradients obtained using the adjoint approach are correct to at least 13 digits of numerical precision.

Table 2 Comparison of the adjoint and complex variable gradients for uncoupled propagation adjoint

Grid point	Complex variable gradient	Adjoint gradient
500	−0.009333018682250	−0.009333018682276
1000	−0.006524286483017	−0.006524286483021
2000	−0.003480798119162	−0.003480798119131
5000	0.000483509101314	0.000483509101372
8000	−0.083586334960307	−0.083586334960355

IV. Coupled Computational-Fluid-Dynamics/Boom-Adjoint Formulation

The coupled adjoint formulation is essentially the same as that introduced in our earlier work [9] and is included here for the sake of completeness. The boom-adjoint formulation is coupled with the NASA Langley unstructured CFD solver FUN3D [18]. The FUN3D software solves the compressible and incompressible forms of the steady and unsteady Euler and Reynolds-averaged Navier–Stokes equations on general static and dynamic mixed-element grid discretizations, which may optionally include overset grid topologies. The software has been used for a broad class of aerodynamic analysis and design simulations across the speed range. FUN3D also offers a discretely consistent adjoint implementation that has been used to perform mathematically rigorous design optimization [13,19,20], error estimation, and formal mesh adaptation [21,22] for complex geometries and flowfields in massively parallel computing environments. These applications include accurate analysis and design optimization of aircraft concepts aimed at sonic-boom mitigation [23,24]. Such simulations have traditionally relied on objective functions posed in the near field within 20 body lengths of the vehicle, ultimately yielding an indirect approach that fails to formally address the pressure signature on the ground. However, the adjoint approach for the propagation methodology developed here offers an exciting opportunity to formally couple existing near-field CFD analysis and design capabilities with the methodology used to predict ground-based metrics. Finally, it should be noted that FUN3D also offers a discretely consistent forward mode of differentiation. A scripting procedure [25] can be used to automatically convert the baseline source code to a complex-variable formulation as described previously. In this manner, sensitivities of all FUN3D outputs with respect to any input parameter may be easily evaluated.

The coupled formulation is described from the perspective of the CFD solver. In this approach, the interface between FUN3D and boom propagation takes the form of a one-dimensional pressure distribution p_0 evaluated at a fixed distance from the aircraft in the near-field CFD mesh. The CFD solution determined on the unstructured mesh is used to construct this pressure distribution, which serves as the input for the boom analysis problem. Given p_0, the forward mode of boom analysis evaluates the cost function l_N. The adjoint mode then determines the sensitivity of the cost function to p_0, which is a horizontal vector denoted $\mathrm{d}l_N/\mathrm{d}p_0$.

The relationship between the near-field pressure signature and the CFD solution is described as

$$p_0 = \mathbf{T}(\boldsymbol{Q}, \boldsymbol{X}) \tag{20}$$

where the vectors $\boldsymbol{Q}$ and $\boldsymbol{X}$ represent the CFD solution and mesh, respectively, and $\mathbf{T}$ is a transformation mapping the CFD solution to the desired pressure distribution p_0. The Lagrangian for the coupled formulation is defined as

$$\mathbf{L}(\boldsymbol{D}, \boldsymbol{Q}, \boldsymbol{X}, \boldsymbol{\Lambda}_f, \boldsymbol{\Lambda}_g, \boldsymbol{\Lambda}_b) = l_N + [\boldsymbol{\Lambda}_g]^T\mathbf{G} + [\boldsymbol{\Lambda}_f]^T\mathbf{R} + [\boldsymbol{\Lambda}_b]^T(p_0 - \mathbf{T}) \tag{21}$$

Here, $\boldsymbol{\Lambda}_f$ and $\boldsymbol{\Lambda}_g$ are adjoint variables corresponding to the discrete CFD flow equations $\mathbf{R}(\boldsymbol{Q}, \boldsymbol{X}, \boldsymbol{D}) = 0$ and CFD grid equations $\mathbf{G}(\boldsymbol{X}, \boldsymbol{D}) = 0$, respectively; $\boldsymbol{\Lambda}_b$ is a vector of adjoint variables associated with the boom interface given by Eq. (20); and $\boldsymbol{D}$ is a vector of design variables. In the current study, the design variables consist of geometric parameters defining the discrete surface grid for the aircraft.

Differentiating the Lagrangian with respect to $\boldsymbol{D}$ and equating the coefficients of $\partial p_0/\partial \boldsymbol{D}$, $\partial \boldsymbol{X}/\partial \boldsymbol{D}$, and $\partial \boldsymbol{Q}/\partial \boldsymbol{D}$ to zero yields the following system of adjoint equations:

$$\left[\frac{\mathrm{d}l_N}{\mathrm{d}p_0}\right]^T + \boldsymbol{\Lambda}_b = 0, \quad \left[\frac{\partial \mathbf{R}}{\partial \boldsymbol{Q}}\right]^T \boldsymbol{\Lambda}_f - \left[\frac{\partial \mathbf{T}}{\partial \boldsymbol{Q}}\right]^T \boldsymbol{\Lambda}_b = 0,$$
$$\left[\frac{\partial \mathbf{G}}{\partial \boldsymbol{X}}\right]^T \boldsymbol{\Lambda}_g + \left[\frac{\partial \mathbf{R}}{\partial \boldsymbol{X}}\right]^T \boldsymbol{\Lambda}_f - \left[\frac{\partial \mathbf{T}}{\partial \boldsymbol{X}}\right]^T \boldsymbol{\Lambda}_b = 0 \tag{22}$$

Recall that the vector $\mathrm{d}l_N/\mathrm{d}p_0$ is computed using the adjoint mode of boom analysis as described in Secs. II and III. Assuming that the adjoint variables satisfy Eq. (22) and that the transformation $\mathbf{T}$ given by Eq. (20) does not explicitly depend on $\boldsymbol{D}$, the desired sensitivity derivatives of the ground signature with respect to the aircraft geometry are then calculated as follows:

$$\frac{\partial \mathbf{L}}{\partial \boldsymbol{D}} = [\boldsymbol{\Lambda}_g]^T \frac{\partial \mathbf{G}}{\partial \boldsymbol{D}} + [\boldsymbol{\Lambda}_f]^T \frac{\partial \mathbf{R}}{\partial \boldsymbol{D}} \tag{23}$$

Note that the computational cost associated with the solution of Eq. (22) is similar to that of their traditional forward-mode counterparts, and the cost required to evaluate Eq. (23) is trivial. In this manner, the approach outlined here ultimately enables a discretely consistent sensitivity analysis to be performed for the coupled system at the cost of a single forward-mode analysis, even for very large numbers of design variables.

V. Initial Mesh and Geometry Parameterization

The adjoint formulation is applied to a supersonic concept shown in Fig. 1. This baseline configuration is the result of earlier optimization using mixed-fidelity [26], reversed-equivalent-area [27] methods. This baseline configuration has also been successfully optimized using nonadjoint methods in other work [6]. The initial mesh for this concept was generated using VGRID [28] and SSGRID [29] and is shown in Fig. 2. This grid-generation approach is a heuristic technique to align the mesh topology a priori with the expected primary off-body shock structures. A more rigorous adjoint-based approach to mesh adaptation [24] for such problems is described in literature.

The CFD grid uses a plane of symmetry along the centerline and contains 16 million nodes and 96 million tetrahedral elements. The surface mesh for the aircraft is parameterized using a free-form shape-deformation tool called BANDAIDS [30]. BANDAIDS provides a compact set of design variables for modifying a discrete surface mesh in the normal direction along with analytic sensitivities required by the discrete adjoint formulation of the near-field CFD problem. All of the components of the baseline, except the flow-through nacelles, are parameterized and are allowed to vary in the shape optimization exercise. The intersections between aircraft components are held fixed for simplicity, although this is not a requirement of the formulation. The parameters for shape modification are NURBS control points. However, to make smooth changes to the underlying mesh, multiple control points are grouped into a single design variable for the optimizer to modify. For example, all of the control points at constant x sections of the fuselage are grouped into a single variable to allow radial expansion or contraction of that fuselage station. When intersections are present at any particular cross section, multiple control-point groupings per cross section are done making sure the intersection between components is not altered. The pod control points are grouped along constant x sections, the wing and horizontal tail control points are grouped along the constant y sections, vertical tail control points are grouped along constant z sections, and pylon control variables are grouped along sections parallel to its root airfoil. After such control point groupings, there are a total of 143 design variables for modifying the different components of the aircraft concept, but only 92 of them are allowed to change during optimization. Of these 92, 49 are used on the fuselage, five on the pod, 18 on the wing, four on the vertical tail, 12 on the

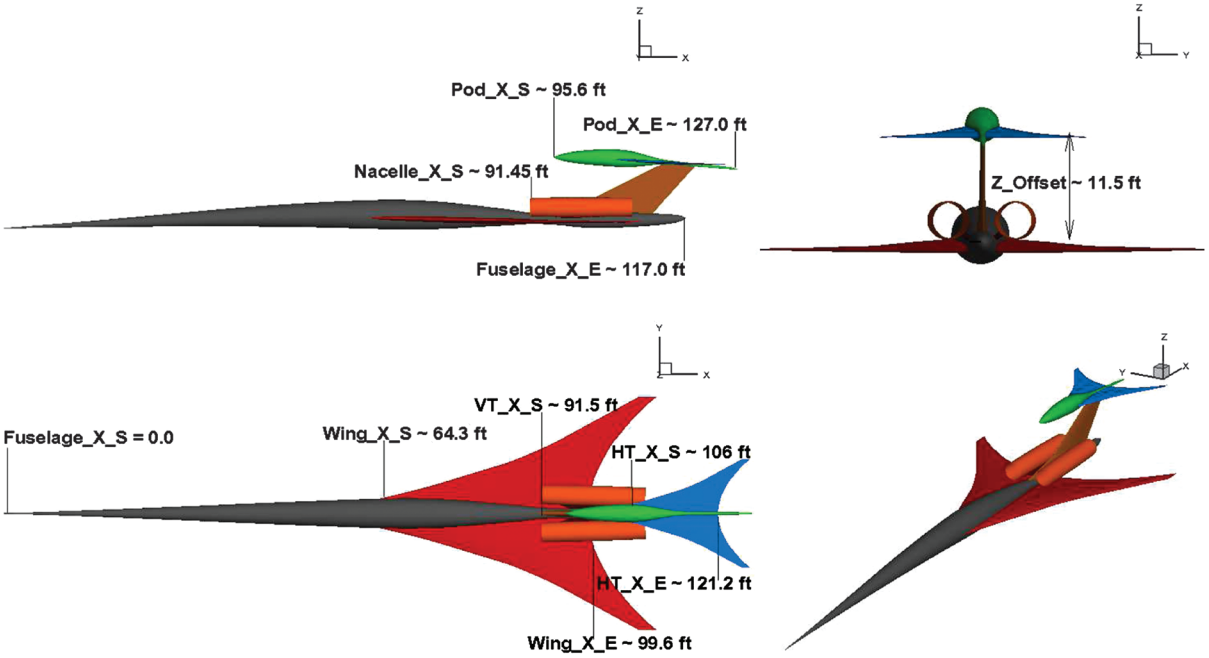

Fig. 1 Orthogonal projections of the baseline configuration.

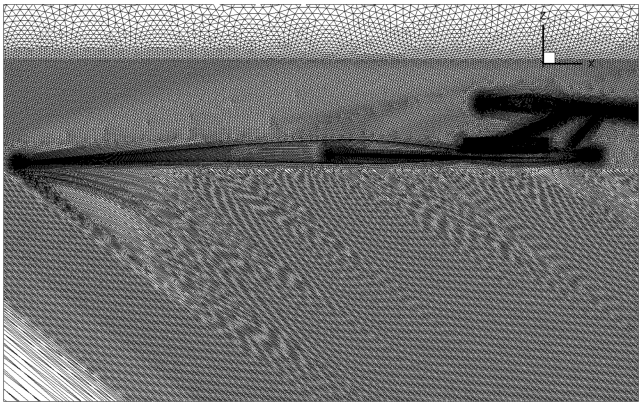

Fig. 2 CFD stretched grid.

horizontal tail, and four on the pylon. These control point groupings are chosen to provide smooth changes to the underlying mesh and geometry. Examples of sample arbitrary deformations over the fuselage, with changes to three fuselage sections and the wing and with changes to five cross sections, are shown in Figs. 3 and 4, respectively. Because of compact support of NURBS basis functions, deformations at any section smoothly deforms the underlying mesh up to two adjacent stations on either side of the location being deformed. The primary criteria in the choice of parameterization was to strike a balance between number of design variables and deformation smoothness. There may exist other parameterizations that satisfy these criteria and may work better, they but were not tried in this study.

Similar to the previous verification cases, the coupled-adjoint sensitivities are compared against complex sensitivities for the coupled problem. The coupled sensitivity values match well up to 13 digits of numerical precision. This is the same accuracy achieved from the propagation adjoint alone; therefore, the coupled problem accuracy match is not expected to be better. Because sensitivities match for several decimal digits, the adjoint sensitivities can be used effectively during numerical optimization.

VI. Computational Results

This section presents the results of the coupled-adjoint formulation for complete configurations in supersonic flow with freestream Mach number of 1.6 and angle of attack of 0.6 deg. The near field was

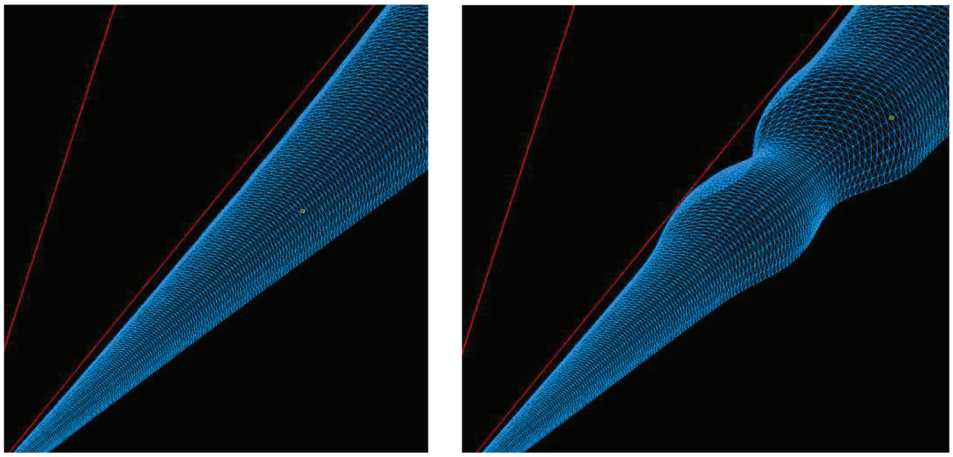

a) Baseline mesh of fuselage nose **b) Modified nose after arbitrary perturbation**

Fig. 3 Arbitrary mesh deformation of fuselage nose.

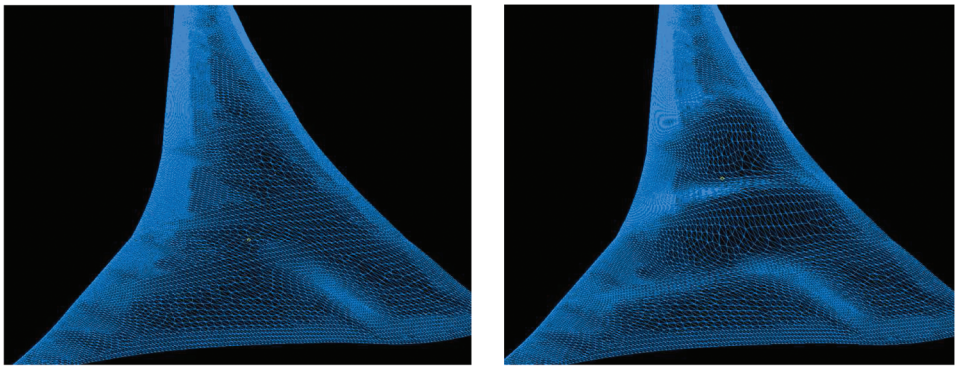

a) Baseline mesh of wing upper surface

b) Modified upper wing after arbitrary perturbation

Fig. 4 Arbitrary mesh deformation of wing upper surface.

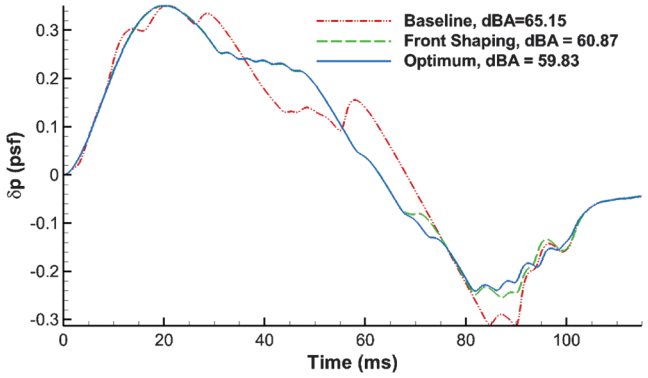

Fig. 5 Ground signature comparison.

extracted at an off-body distance of 381 ft below the aircraft, which translates to three body-lengths. The objective is to reduce the A-weighted loudness of the sonic-boom signatures at the ground level using the squared cost functional given in Eq. (14). Because viscous effects are likely to be small for these configurations when the primary objective is sonic boom, an Euler solver is used for this study.

Optimization was attempted using a flow-through engine setting where the nacelles are almost-constant-area ducts. Different optimization packages (SNOPT [31], NPSOL [32], and PORT [33]) were tried during the course of this study. SNOPT and NPSOL offer gradient-based shape optimization under design constraints, while PORT cannot handle explicit constraints. Although SNOPT and NPSOL were both used to minimize the loudness-based cost functional, PORT generated the best results for the unconstrained optimization problem considered in this study. For sake of brevity, only the results using PORT, are shared and discussed. The choice of the optimizer is problem- and configuration-dependent, and attempting to compare different optimizers is a time-consuming exercise and is not pursued here.

To simplify the problem, as well as to reduce the dimensionality during optimization, the optimization problem is, arbitrarily, broken down into two optimization problems. This is not a general recipe for shape optimization in these kinds of problems; other optimization set-ups might work as well. In the first optimization, the fuselage front portions and wing are shaped to minimize the cost functional. In the second optimization, the aft portions of the fuselage, horizontal tail, vertical tail, pylon, and pod are allowed to vary in their shape in addition to the front fuselage and the wing. The shapes of the front fuselage and wing at the termination of the first optimization are chosen as the initial shapes for the front fuselage and the wing in the second optimization. Even though the components shaped in the first optimization are allowed to vary in the second optimization, because the cost functional sensitivities with respect to the shaped component parameters are close to zero after the first optimization, not much change in observed in their shapes during the second optimization. The number of design variables used is 54 and 92 in the first and second optimizations, respectively.

Figure 5 shows the ground signature of the baseline along with the signatures obtained after each optimization process. During the first optimization, the optimizer successfully smooths out the front portion of the signature and attempts to break up the stronger aft shocks. In the second optimization, the optimizer further refines the aircraft outer mold line to achieve a slightly better ground signature. The A-weighted loudness reduces from a value of 65.15 dBA for the baseline to a value of 59.83 dBA. Table 3 provides other metrics corresponding to these ground signatures. The total perceived loudness drops by around 4.8 dB compared to the baseline; however, there is a small penalty in terms of reduced lift-to-drag ratio. Although the gradient vector at the termination point has nonzero L2 norm, the steepest descent step size needed to make any improvement in the objective functional is less than 10^{-12}. The adjoint gradients were verified to match the complex variable gradients at the termination point, verifying that the gradients are numerically accurate. The norm of the gradient vector when the optimizer terminates is two orders of magnitude smaller than the norm of the gradient vector for the baseline configuration.

The optimizer makes several nonintuitive modifications to the baseline geometry to reduce the A-weighted loudness of the ground signature. The cross-sectional differences between the baseline and the final configuration are shown in Figs. 6 and 7. Figures 6a and 6b show the changes at some cross sections for the wing and horizontal tail, respectively; the spanwise nondimensional distance of each cross section is also listed. In these comparisons, solid lines represent the baseline, while the dashed lines represent the optimum configuration. It is seen that the wing and horizontal tail thicknesses of the optimal configuration is larger than that of the baseline for most sections. The changes to the fuselage and pod at different nondimensional longitudinal locations are shown in Figs. 7a and 7b, respectively. As is evident from Fig. 7a, the intersections between components are not allowed to vary during optimization. Volume is added at the front of the fuselage, while it is removed toward the aft regions. Relatively large changes are observed for the pod geometry.

Figure 8 depicts the near-field pressure distribution comparison. From this plot, it can be seen that the optimizer attempts to reposition the shocks in such a way to maximize shock cancellation through relative placement of shocks and expansion regions. The wing shock structure is redistributed so that the rear shock system is reduced.

Table 3 Comparison of metrics corresponding to the ground signatures

Case	dBA	PLdB	L/D
Baseline	65.15	79.7	7.27
Front shaping	60.87	76.5	7.08
Optimum	59.83	74.9	6.98

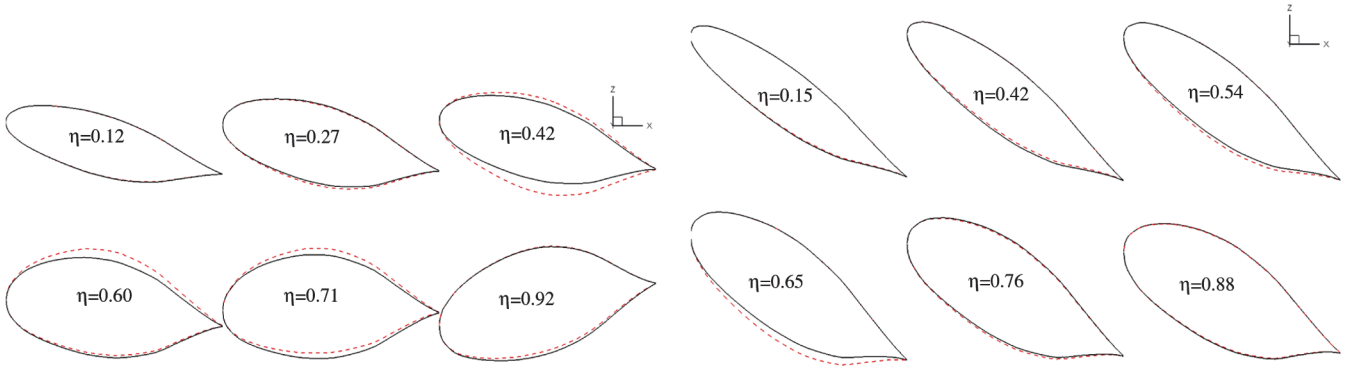

a) Changes to the wing **b) Changes to the horizontal tail**

Fig. 6 Comparison of the cross sections of the baseline and final concept.

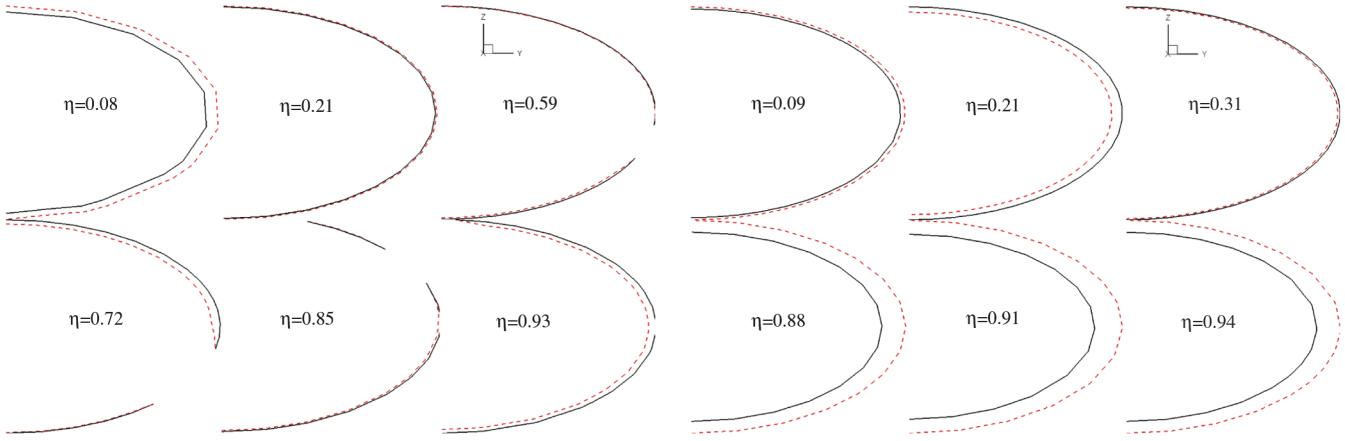

a) Changes to the fuselage **b) Changes to the pod**

Fig. 7 Comparison of the cross sections of the baseline and final concept.

Changing the aft components does not alter the aft shock system significantly; however, small changes are enough to make a significant impact at the ground level in terms of ground signature and loudness levels. The iteration history of the objective function values is plotted in Fig. 9. The optimizer reduces the cost functional (indirectly the A-weighted loudness) from the baseline in two steps. In the first step, significant gains are made in a few design cycles followed by slow and steady progress. The second optimization further reduces the cost functional before optimization is terminated because of termination criteria set at the start of the optimization process.

The computations were carried out on 75 nodes of the SGI ICE X InfiniBand cluster at NASA Ames Research Center. Each node contains dual-socket, eight-core 2.6 GHz Sandy Bridge CPUs, making it 16 cores per node and 32 GB of memory (or 2 GB per core). The computational wall time for this run was about 48 h with 377 flow and 180 adjoint solutions, respectively. The flow solver residual usually drops by six to seven orders of magnitude before declaring convergence, and the adjoint solver residual drops by 12 to 13 orders of magnitude.

Figure 10 depicts the surface sensitivity contours of ground-based cost functional with respect to the normal perturbations to the surface geometry for the baseline and optimal configurations. For undertrack boom metrics, as expected, the lower surface of the aircraft is more sensitive than the upper surface. The adjoint process attempts to make the design parameters associated with the active design variables insensitive to the ground-based cost functional, as evidenced by the larger fraction of green regions in the sensitivity contour spectrum for the optimum design. Overall, the optimal configuration is much less sensitive to the objective than the baseline. Certain locations in the optimal configuration have large sensitivities because these locations are not allowed to vary due of their proximity to intersection regions.

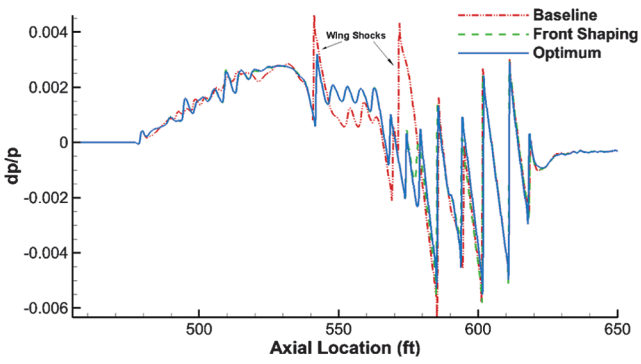

Fig. 8 Baseline and final near-field pressure waveforms.

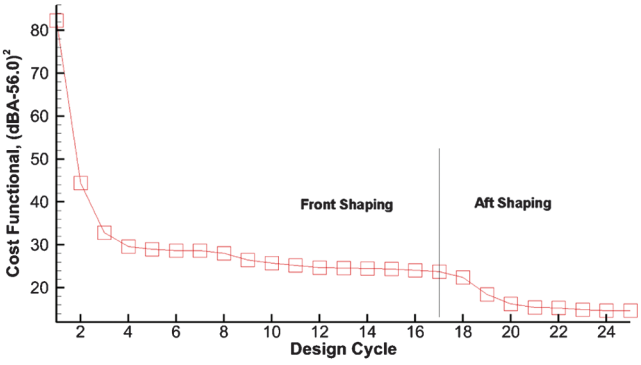

Fig. 9 Iteration history of the optimizer.

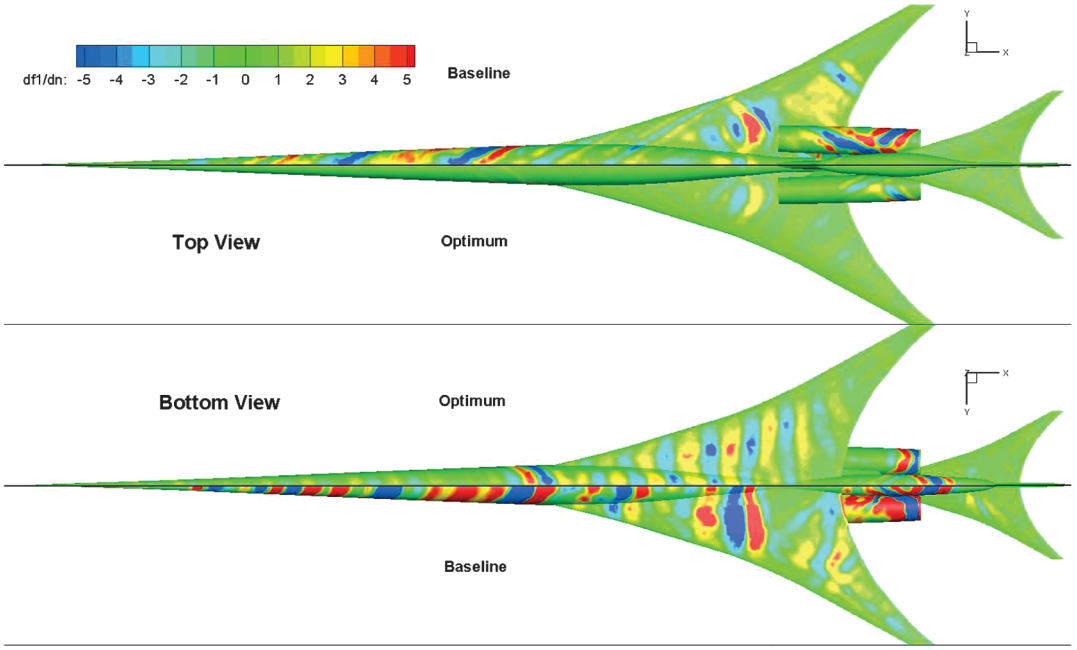

Fig. 10 Comparison of surface sensitivity contours of ground-based cost functional with respect to the normal perturbations to the surface geometry.

These sorts of plots will help in choosing appropriate design variables in the shape optimization process. These figures represent only a snapshot in a dynamically varying sensitivity field; as the design changes, the sensitivity contours change. Future work would have to use this information to constantly update and restrict the active design variables to those that have the highest impact on the cost functional. This will help reduce the number of design variables; however, the complexity of the optimizer will increase due to the additional bookkeeping.

Because gradient-based optimization is a path-building approach, starting from a different initial configuration may lead to a different, possibly better, optimal configuration. However, that does not add any research value to the current effort. Uncertainty can creep into the formulation through various means, mesh quality, parameterization and shape deformation, optimization, and problem formulation, to name a few. Each of these aspects is a research topic in its own right and is beyond the scope of this study. This study successfully demonstrates that adjoint-based shape optimization may be used to directly optimize loudness values of sonic-boom ground signatures by achieving a significant design improvement in terms of loudness. From the perspective of boom loudness, each decibel reduction is extremely crucial; a reduction of 4.8 dB on the perceived loudness scale over an already optimized geometry is considered significant.

It is the belief of the authors that the adjoint-based optimization approaches, including the approach presented here, can complement advanced conceptual design methods. Some of the current outstanding issues include simultaneous adjoint mesh adaptation and design, and improved gradient-based optimization algorithms capable of approaching the global minimum or at least overcoming shallow local minima. Sonic-boom mitigation represents a challenging, highly integrated design problem that can be solved with the right mix of tools that have been introduced here and elsewhere in literature. The challenge is to refine the process such that each contributing analysis is robust and reliable and does not artificially constrain the optimizer in its design space exploration.

VII. Conclusions

A sonic-boom ground signature loudness sensitivity method has been developed using the discrete adjoint approach and the augmented Burgers's equation. The boom-adjoint method has been formally coupled with a high-fidelity CFD and shape-optimization environment for designing low-boom supersonic aircraft concepts. Based on the optimization results for a configuration previously optimized with other state-of-the-art conceptual design methods, significant positive changes to the ground signature were obtained by subtle nonintuitive changes to the aircraft outer mold line. The coupled adjoint-based formulation is available to include engine simulation as well as viscous solutions if needed. Future work will attempt to use advanced algorithms and hybrid strategies to improve the performance of the optimizers. Additionally, adjoint mesh adaptation in conjunction with adjoint-based design will be used as it becomes available.

Appendix: Propagation Matrices

The tridiagonal matrices for the relaxation processes are

$$A^n, \quad A_2^n = \begin{pmatrix} 1 & 0 & \cdots & & \\ 0 & 1 & 0 & \cdots & \\ 0 & -\alpha\kappa_1 - \kappa_2 & (1+2\alpha\kappa_1) & \kappa_2 - \alpha\kappa_1 & \cdots \\ & \ddots & \ddots & \ddots & \\ & & \cdots & 0 & 1 \quad 0 \\ & & \cdots & & 0 \quad 1 \end{pmatrix}$$

$$B^n, \quad B_2^n = \begin{pmatrix} 1 & 0 & \cdots & & \\ 0 & 1 & 0 & \cdots & \\ \alpha'\kappa_1 - \kappa_2 & (1-2\alpha'\kappa_1) & \kappa_2 + \alpha'\kappa_1 & \cdots & \\ & \ddots & \ddots & \ddots & \\ & & \cdots & 0 \quad 1 & 0 \\ & & \cdots & & 0 \quad 1 \end{pmatrix}$$

In the previous matrices

$$\kappa_1 = \frac{C_\nu \Delta\sigma_n}{\Delta\tau^2} \qquad \kappa_2 = \frac{\theta_\nu}{2\Delta\tau}$$

and $\alpha' = 1 - \alpha$. If using the Crank–Nicholson scheme, $\alpha = 0.5$. For thermoviscous absorption, the matrices are given next with

$$\lambda = \frac{\Delta\sigma_n}{2\Gamma(\Delta\tau)^2}$$

$$A_3^n = \begin{pmatrix} 1 & 0 & \cdots & & \\ -\lambda & (1+2\lambda) & -\lambda & \cdots & \\ & \ddots & \ddots & \ddots & \\ & & \cdots & 0 & 1 \end{pmatrix}$$

$$B_3^n = \begin{pmatrix} 1 & 0 & \cdots & & \\ \lambda & (1-2\lambda) & \lambda & \cdots & \\ & \ddots & \ddots & \ddots & \\ & & \cdots & 0 & 1 \end{pmatrix}$$

Acknowledgments

This work was supported by the NASA Project entitled "Sonic Boom Propagation Tools and Methods for Low Sonic Boom Design," under NASA contract number NNL08AA00B, task number NNL12AA55T, through the NASA Fundamental Aeronautics Supersonics Program. The first author wishes to thank Wu Li, Irian Ordaz, and Mike Park for some initial discussions of boom adjoints. The receipt of the time-domain A-weighted loudness calculation code from Gulfstream Aerospace is gratefully acknowledged. The time and effort put in by Scott Brynildsen, Jan-Renee Carlson, Norma Farr, and Dick Campbell for geometry generation and gridding for powered-on engine simulation in a short amount of time and Karl Geiselhart for engine boundary conditions is greatly appreciated. Help in several forms from Lori Ozoroski, Bill Jones, and Bill Kleb is also acknowledged.

References

[1] George, A. R., and Seebass, R., "Sonic Boom Minimization Including Both Front and Rear Shocks," *AIAA Journal*, Vol. 9, No. 10, 1971, pp. 2091–2093. doi:10.2514/3.6478

[2] Seebass, R., "Sonic Boom Reduction Through Aircraft Design and Operation," *11th Aerospace Sciences Meeting*, AIAA Paper 1973-0241, Jan. 1973.

[3] Seebass, R., and George, A., "Sonic Boom Minimization," *Journal of Acoustical Society of America*, Vol. 51, No. 2, 1972, pp. 686–694. doi:10.1121/1.1912902

[4] Pawlowski, J. W., Graham, D. H., Boccadoro, C. H., Coen, P. G., and Maglieri, D. J., "Origins and Overview of the Shaped Sonic Boom Demonstration Program," *43rd AIAA Aerospace Sciences Meeting and Exhibit*, AIAA Paper 2005-0005, Jan. 2005.

[5] Howe, D., Simmons, F., and Freund, D., "Development of the Gulfstream Quiet Spike™ for Sonic Boom Minimization," *46th AIAA Aerospace Sciences Meeting and Exhibit*, AIAA Paper 2008-0124, Jan. 2008.

[6] Ordaz, I., and Li, W., "Adaptive Aft Signature Shaping of a Low-Boom Supersonic Aircraft Using Off-Body Pressures," *50th AIAA Aerospace Sciences Meeting*, AIAA Paper 2012-0020, Jan. 2012.

[7] Nadarajah, S., Jameson, A., and Alonso, J., "Sonic Boom Reduction Using an Adjoint Method for Wing–Body Configurations in Supersonic Flow," *9th AIAA/ISSMO Symposium on Multidisciplinary Analysis and Optimization*, AIAA Paper 2002-5547, Sept. 2002.

[8] Aftosmis, M., Nemec, M., and Cliff, S., "Adjoint-Based Low-Boom Design with Cart3D (Invited)," *29th AIAA Applied Aerodynamics Conference*, AIAA Paper 2011-3500, June 2011.

[9] Rallabhandi, S. K., "Sonic Boom Adjoint Methodology and Its Applications (Invited)," *29th AIAA Applied Aerodynamics Conference*, AIAA Paper 2011-3497, June 2011.

[10] Rallabhandi, S. K., "Advanced Sonic Boom Prediction Using Augmented Burger's Equation," *Journal of Aircraft*, Vol. 48, No. 4, 2011, pp. 1245–1253. doi:10.2514/1.C031248

[11] Cleveland, R. O., "Propagation of Sonic Booms Through a Real, Stratified Atmosphere," Ph.D. Thesis, Univ. of Texas at Austin, Austin, TX, 1995.

[12] Conte, S. D., and deBoor, C., *Elementary Numerical Analysis*, McGraw–Hill, New York, 1972, pp. 153–155.

[13] Nielsen, E. J., Diskin, B., and Yamaleev, N. K., "Discrete Adjoint-Based Design Optimization of Unsteady Turbulent Flows on Dynamic Unstructured Grids," *AIAA Journal*, Vol. 48, No. 6, 2010, pp. 1195–1206. doi:10.2514/1.J050035

[14] Sullivan, B. M., Klos, J., Buehrle, R. D., McCurdy, D. A., and Edward A. Haering, J., "Human Response to Low-Intensity Sonic Booms Heard Indoors and Outdoors," NASA TM-2010-216685, 2010.

[15] Kwon, Y.-H., "Butterworth Digital Filters," 1998, http://www.kwon3d.com/theory/filtering/butt.html [retrieved June 2013].

[16] Lyness, J. N., "Numerical Algorithms Based on the Theory of Complex Variables," *Proceedings of the ACM 22nd National Conference*, ACM, New York, NY, 1967, pp. 124–134.

[17] Lyness, J. N., and Moler, C. B., "Numerical Differentiation of Analytic Functions," *SIAM Journal on Numerical Analysis*, Vol. 4, No. 2, 1967, pp. 202–210. doi:10.1137/0704019

[18] Nielsen, E. J., et al., "FUN3D: Fully Unstructured Navier–Stokes," http://fun3d.larc.nasa.gov [retrieved June 2012].

[19] Nielsen, E., and Diskin, B., "Discrete Adjoint-Based Design for Unsteady Turbulent Flows on Dynamic Overset Unstructured Grids," *50th AIAA Aerospace Sciences Meeting*, AIAA Paper 2012-0554, Jan. 2012.

[20] Nielsen, E. J., and Jones, W. T., "Integrated Design of an Active Flow Control System Using a Time-Dependent Adjoint Method," *Mathematical Modeling of Natural Phenomena*, Vol. 6, No. 3, 2011, pp. 141–165. doi:10.1051/mmnp/20116306

[21] Jones, W. T., Nielsen, E. J., and Park, M. A., "Validation of 3D Adjoint Based Error Estimation and Mesh Adaptation for Sonic Boom Prediction," *44th AIAA Aerospace Sciences Meeting and Exhibit*, AIAA Paper 2006-1150, Jan. 2006.

[22] Park, M. A., Lee-Rausch, E. M., and Rumsey, C. L., "FUN3D and CFL3D Computations for the First High Lift Prediction Workshop," *49th AIAA Aerospace Sciences Meeting*, AIAA Paper 2011-936, Jan. 2011.

[23] Park, M. A., and Darmofal, D. L., "Validation of an Output-Adaptive, Tetrahedral Cut-Cell Method for Sonic Boom Prediction," *AIAA Journal*, Vol. 48, No. 9, 2010, pp. 1928–1945. doi:10.2514/1.J050111

[24] Park, M. A., "Low Boom Configuration Analysis with FUN3D Adjoint Simulation Framework," *29th AIAA Applied Aerodynamics Conference*, AIAA Paper 2011-3337, June 2011.

[25] Kleb, W. L., Nielsen, E. J., Gnoffo, P. A., Park, M. A., and Wood, W. A., "Collaborative Software Development in Support of Fast Adaptive Aerospace Tools (FAAST)," *16th AIAA Computational Fluid Dynamics Conference*, AIAA Paper 2003-3978, June 2003.

[26] Li, W., Shields, E., and Geiselhart, K., "A Mixed- Fidelity Approach for Design of Low-Boom Supersonic Aircraft," *48th AIAA Aerospace Sciences Meeting*, AIAA Paper 2010-0845, Jan. 2010.

[27] Li, W., and Rallabhandi, S. K., "Inverse Design of Low-Boom Supersonic Concepts Using Reversed Equivalent-Area Targets (Invited)," *29th AIAA Applied Aerodynamics Conference*, AIAA Paper 2011-3498, June 2011.

[28] Pirzadeh, S., "Three-Dimensional Unstructured Viscous Grids by the Advancing-Layers Method," *AIAA Journal*, Vol. 34, No. 1, 1996, pp. 43–49. doi:10.2514/3.13019

[29] Campbell, R. L., Carter, M. B., Deere, K. A., and Waithe, K. A., "Efficient Unstructured Grid Adaptation Methods for Sonic Boom Prediction," *26th AIAA Applied Aerodynamics Conference*, AIAA Paper 2008-7327, Aug. 2008.

[30] Samareh, J. A., "Aerodynamic Shape Optimization Based on Free-Form Deformation," *10th AIAA/ISSMO Multidisciplinary Analysis and Optimization Conference*, AIAA Paper 2004-4630, Aug.–Sept. 2004.

[31] Gill, P. E., Murray, W., and Saunders, M., "SNOPT: Software for Large-Scale Nonlinear Programming," June 2008, http://www.sbsi-sol-optimize.com/manuals/SNOPTManual.pdf [retrieved June 2013].

[32] Gill, P. E., and Murray, W., et al., "NPSOL: A Fortran Package for Nonlinear Programming," http://www.sbsi-sol-optimize.com [retrieved June 2013].

[33] Blue, J., Fox, P., and Fullerton, W., et al., "PORT Mathematical Subroutine Library," http://www.bell-labs.com/project/PORT [retrieved June 2013].